Chemistry & Biology
Article

Conformation Sensors that Distinguish Monomeric Proteins from Oligomers in Live Cells

Yasmin M. Ramdzan,[1] Rebecca M. Nisbet,[1] Jason Miller,[2,3] Steven Finkbeiner,[2,4,5] Andrew F. Hill,[1] and Danny M. Hatters[1,*]

[1]Department of Biochemistry and Molecular Biology, The University of Melbourne, Bio21 Molecular Science and Biotechnology Institute and Mental Health Research Institute, Parkville VIC 3010, Victoria, Australia
[2]Gladstone Institute of Neurological Disease and the Taube-Koret Center for Huntington's Disease Research, San Francisco, CA 94158, USA
[3]Medical Scientist Training Program and the Chemistry and Chemical Biology Program
[4]Department of Neurology
[5]Department of Physiology
University of California, San Francisco, San Francisco, CA 94143, USA
*Correspondence: dhatters@unimelb.edu.au
DOI 10.1016/j.chembiol.2010.03.011

SUMMARY

Proteins prone to misfolding form large macroscopic deposits in many neurodegenerative diseases. Yet the in situ aggregation kinetics remains poorly understood because of an inability to demarcate precursor oligomers from monomers. We developed a strategy for mapping the localization of soluble oligomers and monomers directly in live cells. Sensors for mutant huntingtin, which forms aggregates in Huntington's disease, were made by introducing a tetracysteine motif into huntingtin that becomes occluded from binding biarsenical fluorophores in oligomers, but not monomers. Up to 70% of the diffusely distributed huntingtin molecules appeared as submicroscopic oligomers in individual neuroblastoma cells expressing mutant huntingtin. We anticipate the sensors to enable insight into cellular mechanisms mediated by oligomers and monomers and for the approach to be adaptable more generally in the study of protein self-association.

INTRODUCTION

The misfolding of proteins into macroscopic aggregates such as plaques and inclusion bodies is a hallmark of Alzheimer's, Creutzfeldt-Jakob, Huntington's, and other neurodegenerative diseases (Chiti and Dobson, 2006). However, the role of aggregation, per se, in disease is controversial. Indeed, in many of these diseases, notably Huntington's, Alzheimer's, and Parkinson's, small soluble oligomers or other diffuse forms, which may be precursors to the macroscopic aggregates, seem to correlate best with cellular dysfunction (Arrasate et al., 2004; Haass and Selkoe, 2007). Despite evidence that soluble oligomers are more toxic than the macroscopic aggregates, quantitative assessment of the formation of the earliest, submicroscopic oligomers in live cells is limited by the lack of suitable tools. To overcome these limitations, we developed a novel approach to rapidly distinguish monomers from all other soluble aggregates directly in live cells.

Our approach centers on the mutant exon 1 fragment of huntingtin (Htt_{ex1}), which has been used extensively to model Huntington's disease in transgenic mice, mammalian cells, *Drosophila melanogaster*, yeast, and *Caenorhabditis elegans* (Brignull et al., 2006; Duennwald et al., 2006; Jackson et al., 1998; Mangiarini et al., 1996). Huntington's disease is caused by CAG codon duplications in the *Htt* gene that translate into an abnormally long polyglutamine (polyQ) sequence near the N terminus of the protein (MacDonald et al., 1993). The pathogenic polyQ expansions cause Htt to aggregate and redistribute from a diffuse cytosolic pool into inclusion bodies during disease progression. Normally Htt has 7–36 glutamines in the polyQ repeat, while in disease there are 37 or more (MacDonald et al., 1993). The number of glutamines beyond this threshold is highly correlated with earlier onset of disease and the rate of protein aggregation (Chen et al., 2001; Perutz et al., 1994; Scherzinger et al., 1999). PolyQ expansions have been described in at least eight unrelated proteins that also cause disease, suggesting that aggregation of polyQ is concomitant with cellular dysfunction more generally (Zoghbi and Orr, 2000).

Our approach to distinguish Htt_{ex1} monomers from other oligomers relies on genetically tagging the protein with two labels. The first is Cerulean, a brighter, cyan-fluorescent variant of enhanced green fluorescent protein (EGFP) (Rizzo et al., 2004) that detects Htt_{ex1} localization. Htt_{ex1} fused to EGFP has been used to report on polyQ-dependent inclusion body formation and key cellular toxicities associated with that process (Arrasate et al., 2004; Bennett et al., 2007). The second is a tetracysteine (TC) motif, Cys-Cys-Pro-Gly-Cys-Cys, that binds with high affinity (nanomolar dissociation constant) and specificity to the cell-permeable biarsenical dyes FlAsH and ReAsH (Adams et al., 2002). Upon binding to a TC motif, FlAsH (green fluorescence) and ReAsH (red fluorescence) increase in fluorescence up to 50,000-fold; in the unbound state, the dyes are essentially nonfluorescent (Adams et al., 2002).

Developed as small, and hence less structurally disruptive, alternatives to fluorescent proteins, TC tags and biarsenical dyes have also been used to report on protein folding and conformational changes (Coleman et al., 2009; Ignatova and

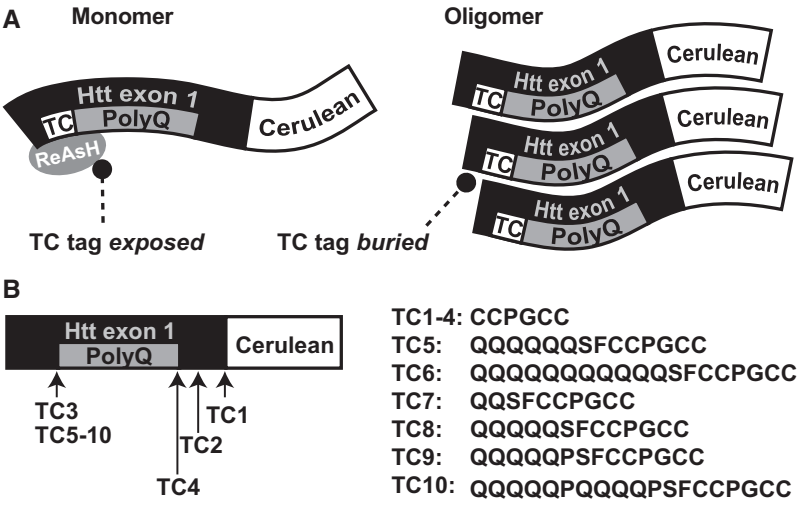

Figure 1. Strategy for Using TC Tags to Demarcate Htt Oligomers from Monomers

(A) The quantity of all forms of Htt_{ex1} is determined from Cerulean fluorescence. ReAsH binding shows whether Htt_{ex1}-Cerulean is aggregated or monomeric.

(B) Schematic of the placement of the TC tags within the Htt_{ex1}-Cerulean sequence and the sequence of the TC insertions. The exact sequence locations are described in detail in Figure S1.

Gierasch, 2004; Luedtke et al., 2007; Roberti et al., 2007). We devised a novel adaptation of the TC motif so that the conversion of Htt_{ex1} monomer into oligomers rendered the TC tag inaccessible to ReAsH. We extended this approach to other color combinations by using Htt_{ex1} fused to the red fluorescent protein Cherry to track Htt_{ex1} localization and the use of FlAsH to selectively label the monomeric forms of Htt_{ex1}. Hence, two-color fluorescence detection for ReAsH reactivity (red) and Cerulean (cyan) or the alternative pair of FlAsH reactivity (green) and Cherry (red) enabled the quantitative monitoring of protein oligomerization directly in situ. Here we describe the development and validation of the approach and its use to visually distinguish monomers from all other oligomers of Htt within living cells.

RESULTS

Development of the Initial Generation of Markers

A single TC tag was initially inserted into the Htt_{ex1}-Cerulean sequence at various locations with the goal of identifying sequence positions in which TC was exposed in Htt_{ex1}-Cerulean monomers and buried in oligomers. Because high-resolution structures of Htt_{ex1} are not available, we used a systematic scanning approach guided by known conformational properties of Htt_{ex1}. Htt_{ex1} monomers sample a series of compact and non-compact conformations with little stable secondary structure, but the polyQ region is predicted to form a highly stable, compact β sheet core in aggregated Htt (Bennett et al., 2002; Crick et al., 2006; Dougan et al., 2009; Perutz et al., 1994). Thus, TC tags inserted near the polyQ region are likely to bind biarsenical dyes in the monomer due to the high solvent accessibility but be inaccessible in oligomers and larger aggregates (Figure 1A). Hence, in our first generation of variants, the TC tag was placed at the junction of Htt and Cerulean (TC1), within the proline-rich region of Htt (TC2), or at the N terminus of the polyQ repeat sequence (TC3) (Figure 1B; see Figure S1A available online).

To test TC1–3 as aggregation reporters, we expressed and purified the recombinant proteins from *Escherichia coli* using a pathogenic polyQ length (Htt_{ex1}^{46Q}) that readily forms amyloid-like fibrils in vitro (Scherzinger et al., 1999). To regulate the rate of aggregation in vitro, we fused Htt_{ex1}^{46Q}-Cerulean to the C terminus of maltose binding protein, which inhibited aggregation in a manner similar to that of Htt_{ex1} fused to glutathione S-transferase (Schaffar et al., 2004; Scherzinger et al., 1999) (Figure 2A). Tobacco etch virus (TEV) protease liberated monomeric Htt_{ex1}^{46Q}-Cerulean, which over time formed aggregates that were insoluble in sodium dodecyl sulfate (SDS) (Figure 2A).

To validate Cerulean as a robust indicator of protein levels regardless of aggregation status, we assessed its fluorescence in soluble protein (monomer) and aggregated states. We found no difference (Figures S2A–S2C), consistent with the ability of EGFP, which is similar to Cerulean in structure and sequence, to report on Htt_{ex1} quantity in cells (Arrasate et al., 2004).

Next, we determined whether the soluble protein or aggregates of each variant of Htt_{ex1}^{46Q}-Cerulean could bind to ReAsH in a native slot blot assay. In this assay, recombinant protein in nondenaturing buffers becomes affixed to a nitrocellulose membrane, while unbound ReAsH passes through (Figure 2B). Htt_{ex1}^{46Q}-Cerulean soluble protein and aggregates without the TC tag bound to the membrane as assessed by Cerulean fluorescence, and ReAsH did not bind appreciably. In contrast, all TC-tagged Htt_{ex1}^{46Q}-Cerulean soluble protein bound to ReAsH (Figure 2B). TC1- and TC2-Htt_{ex1}^{46Q}-Cerulean also bound to ReAsH in the aggregated forms, but TC3-Htt_{ex1}^{46Q}-Cerulean bound poorly, which suggests that TC3 is inaccessible to ReAsH upon aggregation (Figure 1A).

To verify that TC3 reports on aggregation without perturbing the conformation and aggregation potential, we examined the aggregates by negative-staining electron microscopy. The fibrillar architecture of the TC1–3 variants and the non-TC-tagged forms were similar (Figure S3). In an assay monitoring the quantity of pelleted protein, the kinetics of fibril formation were also similar for TC3-Htt_{ex1}^{46Q}-Cerulean and the non-TC counterpart (Figure 3A). Thus, the TC tags have little, if any, influence on the core aggregation properties of Htt_{ex1}^{46Q}-Cerulean into amyloid-like fibrils.

We next assessed the ability of TC3 to report on the aggregation kinetics of Htt_{ex1}-Cerulean, as judged by ReAsH reactivity (Figure 3B). TC3 ReAsH reactivity decreased as the quantity of pelleted aggregates increased, indicating that TC3 demarcates soluble protein from aggregates in constructs of variable polyQ length (Figure 3B).

Implementation of the Initial TC Constructs in Living Cells

To determine whether the TC3 reporter distinguishes monomers from oligomers in live neuroblastoma (Neuro2a) cells (Figure 4A), we assessed in situ ReAsH reactivity with TC3 in

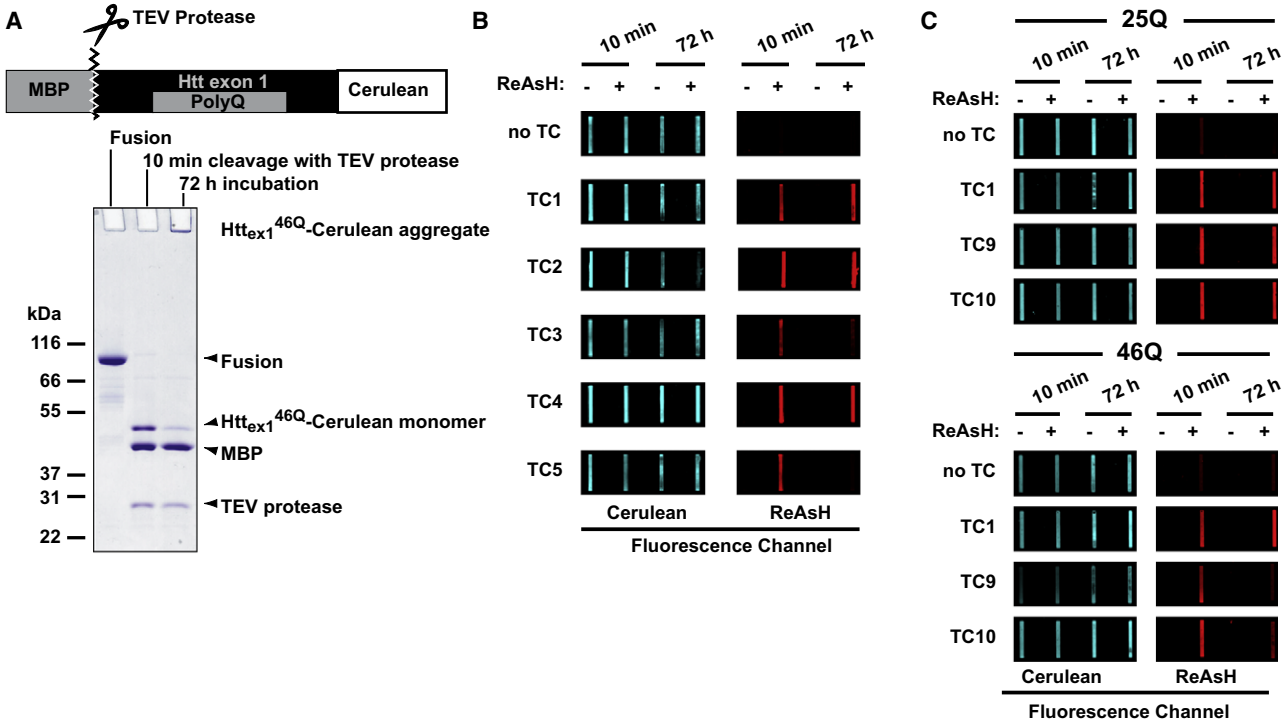

Figure 2. Screening Recombinant Htt$_{ex1}$-Cerulean for ReAsH Reactivity in Monomers versus Aggregates

(A) Fusion of Htt$_{ex1}$-Cerulean to maltose-binding protein (MBP) suppressed aggregation. Aggregation was induced by liberation of MBP with TEV protease, and the efficiency of cleavage was assessed by SDS-PAGE. Aggregates were identified by their insolubility in SDS.

(B) Native slot blots to screen TC-tagged forms of Htt$_{ex1}^{46Q}$-Cerulean for aggregation-dependent ReAsH reactivity. The binding of protein was revealed by Cerulean fluorescence and ReAsH reactivity by ReAsH fluorescence.

(C) Native slot blots to screen for aggregation and polyQ length dependency of ReAsH reactivity for TC1-, TC9-, and TC10-tagged Htt$_{ex1}$-Cerulean.

Htt$_{ex1}^{25Q}$-Cerulean, which has a subpathogenic polyQ length. Untagged (control) Htt$_{ex1}^{25Q}$-Cerulean had a diffuse, cytosolic distribution with no ReAsH fluorescence and no inclusion bodies. The TC1 counterpart had an identical phenotype but had substantial ReAsH reactivity. In contrast, TC3-Htt$_{ex1}^{25Q}$-Cerulean was unexpectedly distributed into small globular structures that bound poorly to ReAsH (Figure 4A). TC3-Htt$_{ex1}^{46Q}$-Cerulean was also distributed into small globular structures, whereas the TC1 and the non-tagged counterparts formed inclusion bodies in many cells, consistent with the expected behavior of the 46Q context (Arrasate et al., 2004).

The first 18 residues of Htt are critical for its cellular localization and targeting to the endoplasmic reticulum and mitochondria (Atwal et al., 2007; Rockabrand et al., 2007; Steffan et al., 2004). Since TC3 lies between residues 17 and 18 of Htt$_{ex1}$, our data suggest that TC3 disrupts normal interactions with cellular components and ligands through this motif. Yet while the kinetics studies of recombinant protein (Figure 3) suggested that this defect is independent of its intrinsic aggregation properties, we cannot exclude the possibility that TC3 changed the aggregation potential of the polyQ sequence in the cellular environment. Indeed, a recent study implicated the first 17 residues

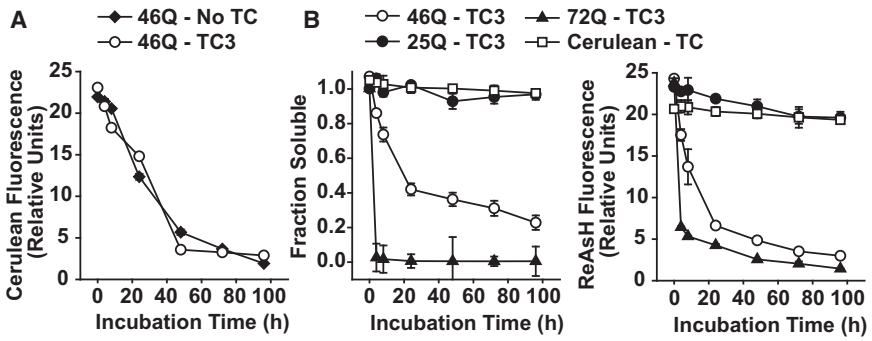

Figure 3. TC3 Reports on Htt$_{ex1}$ Aggregation State In Vitro with No Detectable Alterations in Aggregation Properties

(A) Recombinant TC3-Htt$_{ex1}^{46Q}$-Cerulean aggregates at a rate similar to that of untagged Htt$_{ex1}^{46Q}$-Cerulean; thus, the tag does not interfere with the intrinsic aggregation potential.

(B) PolyQ length dependency of TC3-Htt$_{ex1}$-Cerulean aggregation rates correlates with the extent of ReAsH reactivity, indicating that TC3 does not bind to ReAsH when Htt$_{ex1}$-Cerulean forms aggregates. Cerulean-TC is shown as a non-aggregating control, indicating that a TC motif remains available for ReAsH binding throughout the duration of the experiment. Values are mean ± SD (n = 3).

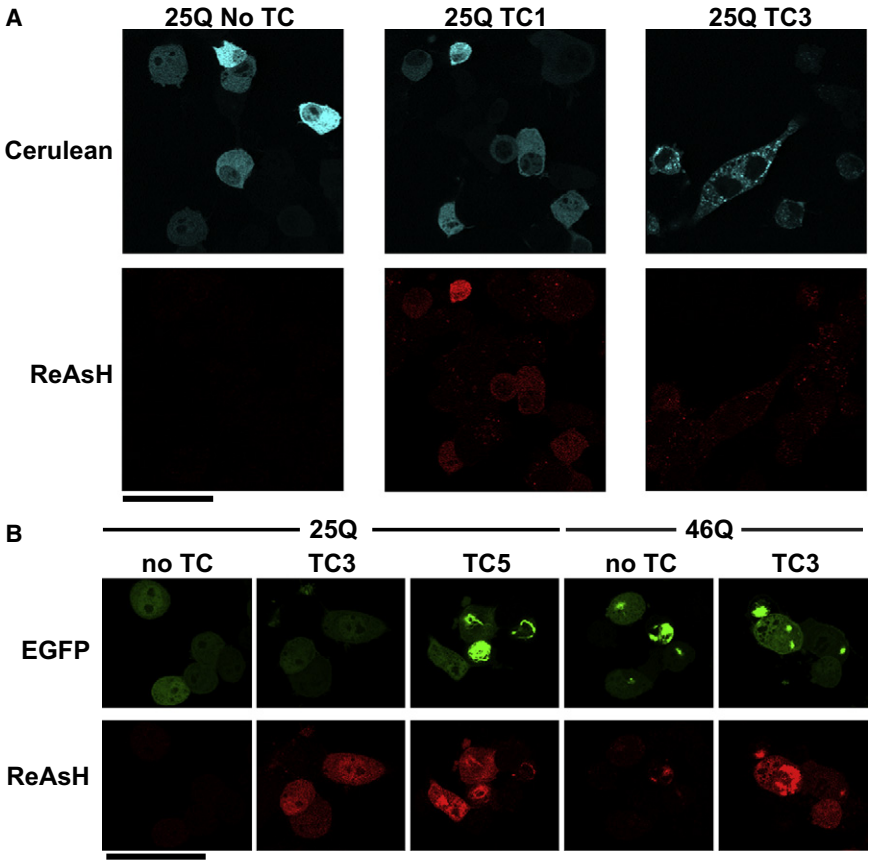

Figure 4. TC3 Interferes with Htt_{ex1}-Cerulean Cellular Localization but Not the In-Cell Aggregation Potential

(A) TC1-Htt_{ex1}^{25Q}-Cerulean and the non-TC counterpart have a diffuse cytosolic localization in neuro2a cells and bind ReAsH in a TC-dependent manner. TC3- Htt_{ex1}^{25Q}-Cerulean is expressed at much lower levels and has a granular distribution, indicating aberrant localization and/or trafficking. The same phenotype was observed in cells expressing TC3-Htt_{ex1}^{46Q}-Cerulean.

(B) Expression of TC3-polyQ and TC5-polyQ lacking other Htt-specific sequences in neuro2a cells. TC3-25Q-GFP and TC3-46Q-GFP displayed aggregation and localization phenotypes identical to those of their non-TC counterparts. In contrast, TC5-25Q-GFP formed inclusions, indicating that polyQ linkers can enhance the in-cell aggregation potential when juxtaposed N-terminally to the TC3 tag. Scale bars, 50 μm.

as important in modulating aggregation rates (Thakur et al., 2009).

Hence, to further investigate the cause of this defect, we introduced TC3 into polyQ25-EGFP and polyQ46-EGFP, which lack Htt-specific sequences other than the polyQ sequence (Figure S1B). TC3 did not influence the localization or inclusion body formation of polyQ25- or polyQ46-EGFP, confirming that TC3 does not intrinsically alter aggregation in cells (Figure 4B). Additionally, ReAsH bound readily to the TC3-polyQ-EGFP constructs, suggesting that TC3 can be adapted to other polyQ-containing proteins.

Refinement of TC3 to Prevent Htt Cellular Localization Defects

To prevent the defects TC3 causes in Htt_{ex1}-Cerulean, we initially tried two approaches. First, since a TC tag reports on oligomerization when juxtaposed to the N terminus of polyQ and might also do so when juxtaposed to the C terminus, we shifted the TC tag outside the first 18 residues of Htt (Figure 1B, TC4). However, in the native slot blot assay, there was no difference in ReAsH reactivity between soluble protein and aggregates of recombinant TC4-Htt_{ex1}^{46Q}-Cerulean (Figure 2B).

Second, we retained the position of TC3 but inserted a new $polyQ_6$ linker sequence immediately N-terminal to the TC tag to restore the 18 residue homology of Htt (Figure 1B, TC5). Recombinant TC5-Htt_{ex1}^{46Q}-Cerulean showed a marked decrease in ReAsH reactivity from soluble protein to aggregate in the native slot blot assay, providing confidence that this second approach might work (Figure 2B). In neuro2a cells, TC5-Htt_{ex1}^{25Q}-Cerulean had a mostly normal cellular distribution; however, approximately 25% cells also displayed a more punctate cellular distribution, suggesting that the linker did not fully rescue the defects of TC3 (Figure S4A).

Next, we extended the linker sequence before TC3 from 6Q in TC5 to 11Q (TC6), a polyQ repeat length comparable to the shortest natural variants in human Htt (Zuhlke et al., 1993) (Figure 1B). To our surprise, TC6-Htt_{ex1}^{25Q}-Cerulean, which has an 11Q sequence followed by the TC tag and endogenous 25Q sequence, formed inclusion bodies in many cells (Figure S4A), perhaps because the new polyQ sequence N-terminal to TC3 increases the aggregation potential of the endogenous polyQ sequence. To determine if the enhanced inclusion body formation was independent of Htt_{ex1}-specific trafficking defects caused by TC3, we introduced TC5 into polyQ25-EGFP. TC5-polyQ25-EGFP had a phenotype similar to that of TC5 in the Htt_{ex1}-Cerulean context, confirming that the enhanced aggregation is independent of the localization defects (Figure 4B).

We also investigated whether shortening the linker would reduce the aggregation potential without causing mislocalization (two or five glutamines; Figure 1B, TC7 and TC8, respectively). TC7 displayed the same defect as TC3, indicating that at least the first 19 residues of Htt are necessary for normal cellular localization; however, TC8-Htt_{ex1}^{25Q}-Cerulean was mostly normally distributed, but over time did form punctate aggregates, albeit to a lesser extent than TC5 and TC6 (Figure S4A).

Nuclear magnetic resonance studies have shown that a TC tag forms a β hairpin centered around the Pro-Gly residues when complexed to ReAsH, suggesting that TC tags stabilize a polyQ hairpin configuration that favors aggregation (Madani et al., 2009). Repeating short polyQ sequences separated by Pro-Gly β hairpins synergistically promote aggregation to a similar or greater extent than the contiguous polyQ sequence lacking the

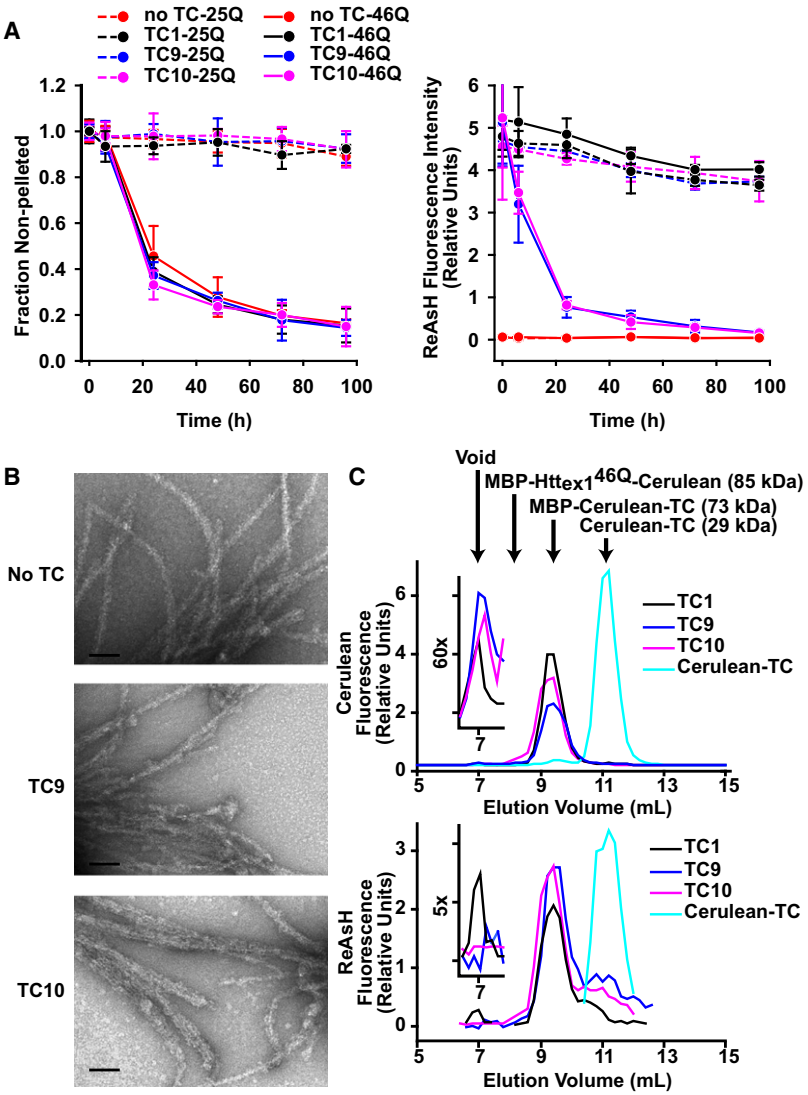

Figure 5. TC9 and TC10 Bind ReAsH Only in Htt Monomers In Vitro with No Detectable Alterations in Aggregation Properties

(A) TC1-, TC9-, and TC10-Htt_{ex1}-Cerulean in the 46Q and 25Q contexts had the same rates of aggregation as their non-TC counterparts when assessed by amount of pelleted material by centrifugation. Thus, the tags do not perturb the intrinsic aggregation potential of Htt_{ex1}. ReAsH reactivity of TC9- and TC10-Htt_{ex1}^{46Q}-Cerulean also correlated with the proportion of non-pelleted material in a microcentrifuge assay, indicating that these tags report on aggregation. In contrast, TC1-Htt_{ex1}^{46Q}-Cerulean showed no decrease or correlation of ReAsH reactivity with non-pelleted material, indicating the ability to bind ReAsH in monomers and aggregates equivalently. Values are mean ± SD (n = 3).

(B) TC9- and TC10-Htt_{ex1}-Cerulean had the same fibrillar morphology as their non-TC counterparts, as assessed by negative-staining electron microscopy. Scale bars, 100 nm.

(C) Gel-filtration chromatography of TC1-, TC9-, and TC10-Htt_{ex1}^{46Q}-Cerulean after 6 hr of incubation. The predominant species eluted at 9.5 ml and likely corresponds to monomers; a small peak at 7 ml corresponds to soluble aggregates. The insets show magnified regions corresponding to the void volume. Arrows point to the elution volume of the proteins indicated above them.

β hairpins (Thakur and Wetzel, 2002). Conversely, aggregation is inhibited when the Pro-Gly β hairpins are replaced with a single Pro residue, which by itself destabilizes configurations favorable for aggregation (Thakur and Wetzel, 2002). To inhibit this mode of TC-facilitated aggregation, we inserted a polyQ linker necessary for proper Htt trafficking (5Q) flanked at the C terminus by a single Pro, immediately N-terminal to the TC3 tag (Figure 1B, TC9). We also examined a construct containing a tandem polyQ5-proline-polyQ4-proline immediately N-terminal to the TC3 tag (Figure 1B, TC10). In neuro2a cells, both TC9- and TC10-Htt_{ex1}-Cerulean showed a normal cellular distribution indistinguishable from that of untagged versions for both the 25Q and 46Q contexts, indicating that we had both rescued the localization defect and prevented TC-facilitated aggregation (Figure S4B).

To validate TC9 and TC10 as aggregation reporters, we examined recombinant TC9- and TC10-Htt_{ex1}-Cerulean for ReAsH reactivity of soluble protein versus aggregates in the native slot blot assay. TC9 and TC10 bound ReAsH in soluble protein (25Q and 46Q) but bound ReAsH poorly as aggregates (46Q) (Figure 2C). TC9 and TC10 also tracked Htt aggregation kinetics by ReAsH reactivity, whereas TC1, whose ReAsH reactivity is insensitive to aggregation state, did not (Figure 5A). TC9 and TC10 did not influence aggregate morphology (Figures 5A and 5B). Furthermore, TC1 and TC9 reported on aggregation similarly with the green fluorescent biarsenical dye FlAsH, indicating that both of the most commonly used biarsenical dyes can be used to demarcate monomers from oligomers (Figure S5).

To determine precisely which oligomeric forms of TC9- and TC10-Htt_{ex1}^{46Q}-Cerulean bind ReAsH, we subjected recombinant TC1-, TC9-, and TC10-tagged Htt_{ex1}^{46Q}-Cerulean to gel-filtration chromatography. After a 6 hr aggregation, the intermediate time point for aggregation kinetics, approximately 5%–10% of Htt_{ex1}^{46Q}-Cerulean, consisted of material that pelleted by centrifugation (Figure 5A). Low-speed pelleting (1500 × g, 5 min) was used to remove the largest aggregates that cannot traverse the Superdex 75 column, and the remaining soluble material was assessed for oligomeric size. The predominant species eluted at a time point consistent with the monomer (Figure 5C). However, a small amount of higher-mass material was found in the void volume, which likely comprises non-pelleted oligomers or material that had self-associated during the chromatography fractionation. Fractions corresponding to eluted protein were assessed for ReAsH reactivity and the TC1, TC9, and TC10 monomer fractions all bound ReAsH. In contrast, only TC1-tagged Htt_{ex1}^{46Q}-Cerulean eluting in the void volume bound ReAsH. The absence of TC9 and TC10 binding to the oligomers in the void volume indicates that the

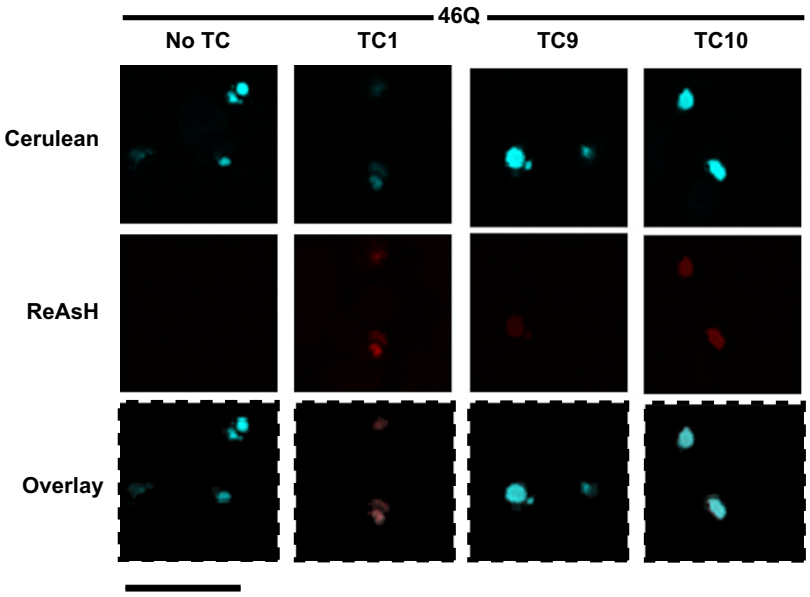

Figure 6. Assessment of TC Tag Reactivity and Detection of Htt_{ex1} Aggregation State within Inclusions

The fluorescence of ReAsH and Cerulean is scaled to emphasize the inclusions (the fluorescence for the other cellular regions are too dim to see). Scale bar, 10 μm. The same images are shown at a lower magnification in Figure S6.

smallest detectable aggregates cannot bind ReAsH. This finding supports the conclusion that TC9 and TC10 binds ReAsH only in monomers, whereas TC1 binds ReAsH similarly in monomers, oligomers, and pelleted aggregates (Figure 5C).

The TC1, TC9, and TC10 constructs were used to examine the extent of aggregation of Htt_{ex1}-Cerulean in neuro2a cells. We first focused on inclusion bodies formed by Htt_{ex1}^{46Q}-Cerulean (Figure 6). TC9 and TC10 showed far less ReAsH reactivity than TC1, which is consistent with inclusion bodies consisting primarily of aggregates (Kim et al., 2002). In Htt_{ex1}^{25Q}-Cerulean, TC1, TC9, and TC10 all bound ReAsH similarly as indicated by tight colocalization of Cerulean and ReAsH fluorescence intensities, consistent with all tags being accessible to bind ReAsH and a lack of oligomers in the cytosol (Figure 7).

We next focused on the cytosolic pool of Htt_{ex1}^{46Q}-Cerulean. TC1 bound ReAsH to about the same extent as it did in Htt_{ex1}^{25Q}-Cerulean (Figure 7). In contrast, TC9 and TC10 showed markedly less ReAsH reactivity than TC1 in the context of Htt_{ex1}^{46Q}-Cerulean and TC9 and TC10 in the context of Htt_{ex1}^{25Q}-Cerulean (Figure 7). Thus, the diffuse pool of cytosolic Htt_{ex1}^{46Q}-Cerulean

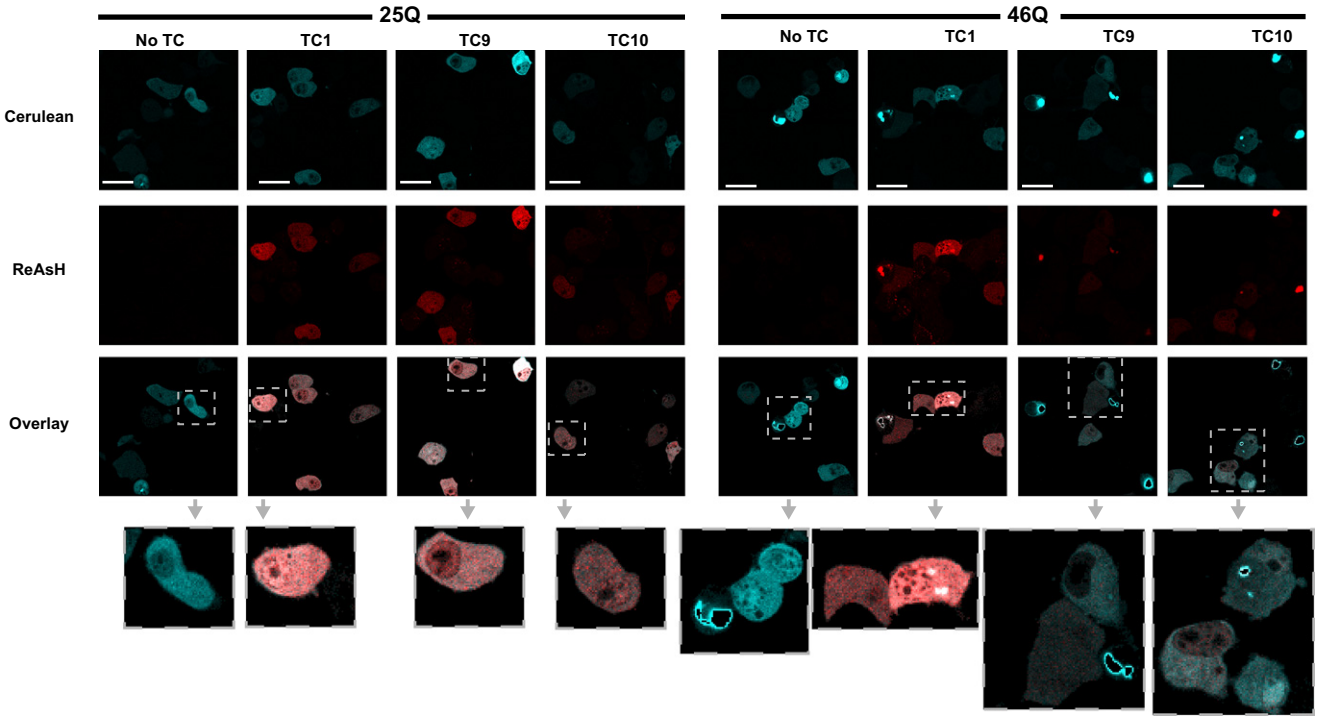

Figure 7. In-Cell Demarcation of Monomers from Oligomers of Htt in Cellular Regions outside of Inclusion Bodies

Images were acquired with the dynamic range adjusted to quantify cytosolic Htt_{ex1}-Cerulean outside inclusion bodies. Note that the inclusion bodies are brighter than the dynamic range of detection and are excluded in the overlay images. Also excluded is Cerulean fluorescence intensity lower than three times the background level. Scale bars, 25 μm. The insets show the selected cells at higher resolution.

evidently comprises a large, evenly distributed proportion of oligomers that are otherwise not visible by confocal microscopy. Analysis of pixel intensity correlation plots and ReAsH fluorescence standardized to the Cerulean fluorescence intensity indicated that the binding of ReAsH to cytosolic TC9- and TC10-Htt_{ex1}^{46Q} was approximately 50%–70% less than the binding of ReAsH to TC9- and TC10-Htt_{ex1}^{25Q}-Cerulean in individual cells (Figure S7A).

We also examined whether FlAsH could be similarly used to report on aggregation in live cells. While FlAsH did bind to TC1- and TC9-Htt_{ex1}-Cerulean, data was difficult to interpret due to a highly efficient FRET from Cerulean to bound FlAsH. Hence, while FRET may have a useful application in the study of Htt conformations, it hinders the utility of Cerulean as an independent marker of protein localization and concentration. To further explore the use of FlAsH to report on Htt_{ex1} aggregation, we replaced the Cerulean moiety with the monomeric red fluorescent protein Cherry. The Cherry/FlAsH labeling combination produced the same result as the Cerulean/ReAsH, validating its use as an alternative spectral toolset for imaging (Figure S7B). Examination of cell-cell differences in ReAsH (or FlAsH) reactivity using the TC9- and TC10-Htt_{ex1}^{46Q}-Cerulean (or Cherry) suggested that different cells have different proportions of cytosolic aggregate/monomer content. In several cells that contained a small inclusion body, overall biarsenical dye reactivity for the cytosolic pool of protein was lower than in neighboring cells (Figure 7 and Figure S7B). Other cells devoid of inclusion bodies also had lower biarsenical dye reactivity than neighboring cells, which raises the possibility that these cells are on track to forming an inclusion (Figure S7B).

DISCUSSION

The development of TC tags as sensors to monitor protein self-association by TC burial has provided a novel means to distinguish between monomers and higher-order oligomers directly in live cells. Here we showed that this approach can be used for FlAsH (green) or ReAsH (red) as sensors of monomers and with Cerulean (cyan) or Cherry (red) as markers of protein localization. Indeed, the ability to monitor the proportion of monomeric relative to oligomeric or microscopically aggregated Htt in situ will be a powerful toolset for investigating how oligomers form, how they are trafficked, and how they relate to inclusion body formation and cellular dysfunction.

A key application of the huntingtin sensors will be in deciphering the precise molecular steps that lead to aggregation and inclusion formation within living cells. The formation of classic inclusions, often used as an indicator of overall aggregation, is a complex cell-mediated process driven by dynein-mediated retrograde transport of misfolded proteins or microaggregates (Kopito, 2000). The nature and toxicity of the forms of protein that precede inclusion formation are largely unknown. However, different aggregation-prone proteins (e.g., SOD1 mutants, PABPN1, and pathogenic Htt_{ex1}) form inclusions with distinct biophysical properties or cellular localizations, suggesting that multiple cellular mechanisms exist to process misfolded or soluble oligomers of proteins (Berger et al., 2006; Matsumoto et al., 2006). In support of this hypothesis, accessory proteins in yeast, such as Bmh1 and Cdc48, alter the intracellular distribution of aggregates and/or inclusion formation (Wang et al., 2009). Moreover, misfolded proteins have been reported to partition into two distinct quality-control compartments that appear visually as inclusions—a juxtanuclear compartment where soluble misfolded proteins are concentrated and a perivacuolar compartment for terminally aggregated proteins (Kaganovich et al., 2008).

In combination, the TC1, TC9, and TC10 markers suggested that the cytosolic pool of Htt_{ex1}^{46Q} had a high proportion of oligomers in many cells (50%–70% in Figure 7; Figure S7) expressing the pathogenic form of Htt_{ex1}, even some cells lacking inclusion bodies. Hence, Htt_{ex1} aggregation appears to occur evenly first in the cytosol before trafficking to inclusions. This conclusion is similar to that reached for a FRET study of another polyQ-containing protein, truncated atrophin-1, whereby pathogenic polyQ lengths induced more oligomers in the cytosol than their non-pathogenic counterpart (Takahashi et al., 2008). These findings highlight a disconnect between visible inclusions and microscopic aggregation and raise the possibility that in disease cellular activities are compromised by pools of oligomers, supporting the notion that inclusions are a protective response by cells to sequester diffuse oligomers.

However, while our data are consistent with Htt_{ex1} forming evenly distributed oligomers in the cytosol, we cannot entirely exclude the possibility that pathogenic Htt_{ex1} acquires a novel monomeric conformation non-permeable to ReAsH binding. This hypothesis is supported by the finding that monomers of polyQ fusions to thioredoxin convert from an α-helical to more compact β sheet conformer before conversion into amyloid-like fibrils (Nagai et al., 2007). In addition, Htt_{ex1} monomers collapse into a more compact conformation immediately after cleavage from glutathione S-transferase, which, like maltose-binding protein, inhibits Htt aggregation (Schaffar et al., 2004). These and other results suggest that monomeric huntingtin, while lacking regular secondary structure, does sample a range of partially compact conformers (Crick et al., 2006; Dougan et al., 2009).

SIGNIFICANCE

The work is significant for two reasons. First, our study shows soluble oligomers of mutant Htt, constituting up to 70% of the diffuse huntingtin molecules, which are otherwise not discernable from monomers by conventional confocal microscopy, to be evenly distributed in the cytosol of many cells and are distinct to the visible inclusion bodies. Hence, small soluble aggregates of Htt are likely to confer a profound burden on cellular functioning in a manner uncorrelated to inclusion bodies, which have been previously postulated to play a direct role in Htt toxicity (reviewed in Hatters, 2008). The second significance is that we describe a new use of TC tags for reporting on protein self-association directly in live cells. The TC tags only bind ReAsH and FlAsH in monomers due to ReAsH occlusion upon oligomerization, which enables monomers to be quantitatively demarcated from oligomers in situ in live cells when used in tandem with a fluorescent protein reporter for localization. This methodology, which we refined for Htt, should be readily adaptable to the other proteins containing polyQ,

enabling insight to be gained as to the role of oligomers in the eight other diseases caused by polyQ expansions. Furthermore, we anticipate the fundamental TC burial methodology to be useful in the study of other proteins that undergo oligomerization as a part of normal cellular biology or with proteins associated with misfolding- and aggregation-related disorders, such as Alzheimer's, Creutzfeldt-Jakob, and Parkinson's.

EXPERIMENTAL PROCEDURES

The cloning of the constructs, the expression and purification of recombinant protein, and the preparation of monomeric Htt_{ex1}-Cerulean or Cerulean-TC are described in the Supplemental Experimental Procedures.

Native Slot Blot Assay

Aliquots of TEV-cleaved fusion proteins (2 μM fusion protein) were either freshly thawed from −80°C storage (10 min TEV cleaved samples) or previously thawed and incubated at 37°C for 72 hr under mineral oil (72 hr samples) prior to analysis. Samples of protein were diluted to a final concentration of 0.8 μM and volume of 100 μl in TNBT buffer [20 mM Tris, 150 mM NaCl, 250 μM BAL (2, 3-dimercapto-1-propanol), and 1 mM tris-carboxyethyl-phosphine (TCEP) (pH 7.4)] with or without 1 μM ReAsH (Invitrogen), which was added from a freshly prepared 2 μM working stock in TNBT. The protein was incubated for 30 min at room temperature and filtered through a nitrocellulose membrane (0.2 μm pore size) using an SF microfiltration unit (Bio-Rad; filtration takes less than 2 min). The sample slots were washed twice by filtration with 100 μl of TNBT buffer and immediately scanned for Cerulean fluorescence (488 nm excitation and 528 nm emission) and ReAsH fluorescence (633 nm excitation and 670 nm emission) with a Typhoon scanner (GE Biosciences).

Pelleting and ReAsH/FlAsH Binding Assays

Aliquots (200 μl) of TEV-cleaved fusion protein (2 μM) in TNBT were thawed, incubated under mineral oil at 37°C for various times, and divided in half. One half was centrifuged at 18,000 × g for 30 min at room temperature, and the supernatant (50 μl) was removed and added to a black-bottomed fluorescence microplate containing 100 μl of TNIT (50 mM Tris, 150 mM NaCl, 12.5 mM imidazole, and 1 mM TCEP). A portion of the uncentrifuged half (50 μl) was added to the microplate as a control for total protein. The samples were analyzed for Cerulean fluorescence intensity (434 nm excitation and 475 nm emission; 5 nm bandwidth) with a fluorescence plate reader (Varioskan; Thermo Electron Corporation).

For ReAsH/FlAsH reactivity, samples were prepared in the same fashion as the noncentrifuged protein except that 150 μl TNIT buffer containing 1.33 μM ReAsH or FlAsH was added to the microplate to provide a final biarsenical dye concentration of 1 μM when the 50 μl protein was added. After a 20 min incubation at room temperature, ReAsH fluorescence (593 nm excitation and 650 nm emission; 5 nm bandwidth) or FlAsH fluorescence (519 nm excitation and 540 nm emission; 5 nm bandwidth) was measured with a fluorescence plate reader (Varioskan).

Transmission Electron Microscopy

Protein samples (2.5 μM) were negatively stained with 1% (w/v) uranyl acetate. Images were collected on a TF30 electron microscope (FEI) fitted with a US1000 2k × 2k CCD camera (Gatan).

Mammalian Cell Culture, ReAsH/FlAsH Staining, and Imaging

Neuro-2a cells were maintained in OptiMem (Invitrogen) supplemented with 10% fetal calf serum, 1 mM glutamine, 100 U/ml penicillin, and 100 μg/ml streptomycin in a humidified incubator with 5% atmospheric CO_2.

For imaging, 8×10^4 cells were plated into a tissue culture-treated 8 well μ-slide (Ibidi). The next day, cells were transfected with the pcDNA3.2 vectors with Lipofectamine 2000 according to the manufacturer's instructions (Invitrogen). The following day, the medium was replaced and the cells were cultured for 24 hr, rinsed twice with 300 μl of pre-warmed HBSS buffer (Invitrogen), and labeled for 30 min with pre-warmed HBSS containing 1 μM ReAsH or FlAsH and 10 μM EDT at 37°C. The cells were washed in pre-warmed HBSS containing 250 μM BAL for 15 min, and the solution was replaced with pre-warmed HBSS.

The cells were imaged live on a TCS SP2 Leica confocal microscope with an HCX PL APO CS 40.0 × 1.25 or HCX PL APO lbd.BL 63 × 1.40 objective, 1 Airy pinhole, and at a scan rate of 200 Hz with four line averages. Cerulean fluorescence was collected at an excitation wavelength of 458 nm and emission wavelengths of 470–520 nm. GFP fluorescence was measured with an excitation laser of 488 nm and emission wavelengths of 500–538 nm. Cherry fluorescence was measured with an excitation laser of 543 nm and emission wavelengths of 575–640 nm. ReAsH fluorescence was collected at an excitation wavelength of 543 nm and emission wavelengths of 580–640 nm. FlAsH fluorescence was collected at an excitation wavelength of 488 nm and emission wavelengths of 500–540 nm. The PMT voltage was kept constant within each experiment and varied between some experiments to optimize signal/noise. Data were obtained in 12 bit format and analyzed with ImageJ. Masks for filtering Cerulean fluorescence were created with a Cerulean threshold range from three times the background fluorescence intensity up to, and excluding, the maximum (i.e., saturated) pixel values. For Cherry, the mask threshold range was from twice the background fluorescence up to, and excluding, the maximum pixel value. Data were corrected for background fluorescence before the ReAsH/Cerulean ratio images were calculated. For the pixel correlation plots, images were converted to 8 bit after data rescaling (to the same scale for multiple images within each experiment) and analyzed with the Image Correlator plugin.

SUPPLEMENTAL INFORMATION

Supplemental Information includes seven figures and Supplemental Experimental Procedures and can be found with this article online at doi:10.1016/j.chembiol.2010.03.011.

ACKNOWLEDGMENTS

We thank K. Goldie for performing the electron microscopy experiments. This work was funded by grants to A.F.H. (National Health and Medical Research Council program grant 400202 and Career Development Award [Level 2] 509400) and D.M.H. (National Health and Medical Research Council project grant 566640). D.M.H. is a CR Roper Fellow. S.F. was supported by the National Institutes of Neurological Disease and Stroke (R01 2NS039074 and R01 2NS045191), the CHDI Foundation, and the Taube-Koret Center for Huntington's Disease Research. J.M. is supported by a predoctoral fellowship from the Hillbloom Foundation as well as the NIH-NIGMS UCSF Medical Scientist Training Program.

Received: September 16, 2009
Revised: March 10, 2010
Accepted: March 19, 2010
Published: April 22, 2010

REFERENCES

Adams, S.R., Campbell, R.E., Gross, L.A., Martin, B.R., Walkup, G.K., Yao, Y., Llopis, J., and Tsien, R.Y. (2002). New biarsenical ligands and tetracysteine motifs for protein labeling *in vitro* and *in vivo*: synthesis and biological applications. J. Am. Chem. Soc. *124*, 6063–6076.

Arrasate, M., Mitra, S., Schweitzer, E.S., Segal, M.R., and Finkbeiner, S. (2004). Inclusion body formation reduces levels of mutant huntingtin and the risk of neuronal death. Nature *431*, 805–810.

Atwal, R.S., Xia, J., Pinchev, D., Taylor, J., Epand, R.M., and Truant, R. (2007). Huntingtin has a membrane association signal that can modulate huntingtin aggregation, nuclear entry and toxicity. Hum. Mol. Genet. *16*, 2600–2615.

Bennett, E.J., Shaler, T.A., Woodman, B., Ryu, K.-Y., Zaitseva, T.S., Becker, C.H., Bates, G.P., Schulman, H., and Kopito, R.R. (2007). Global changes to the ubiquitin system in Huntington's disease. Nature *448*, 704–708.

Bennett, M.J., Huey-Tubman, K.E., Herr, A.B., West, A.P., Jr., Ross, S.A., and Bjorkman, P.J. (2002). A linear lattice model for polyglutamine in CAG-expansion diseases. Proc. Natl. Acad. Sci. USA *99*, 11634–11639.

Berger, Z., Davies, J.E., Luo, S., Pasco, M.Y., Majoul, I., O'Kane, C.J., and Rubinsztein, D.C. (2006). Deleterious and protective properties of an aggregate-prone protein with a polyalanine expansion. Hum. Mol. Genet. *15*, 453–465.

Brignull, H.R., Morley, J.F., Garcia, S.M., Morimoto, R.I., Kheterpal, I., and Wetzel, R. (2006). Modeling polyglutamine pathogenesis in *C. elegans*. Methods Enzymol. *412*, 256.

Chen, S., Berthelier, V., Yang, W., and Wetzel, R. (2001). Polyglutamine aggregation behavior *in vitro* supports a recruitment mechanism of cytotoxicity. J. Mol. Biol. *311*, 173–182.

Chiti, F., and Dobson, C.M. (2006). Protein misfolding, functional amyloid, and human disease. Annu. Rev. Biochem. *75*, 333–366.

Coleman, B.M., Nisbet, R.M., Han, S., Cappai, R., Hatters, D.M., and Hill, A.F. (2009). Conformational detection of prion protein with biarsenical labeling and FlAsH fluorescence. Biochem. Biophys. Res. Commun. *380*, 564–568.

Crick, S.L., Jayaraman, M., Frieden, C., Wetzel, R., and Pappu, R.V. (2006). Fluorescence correlation spectroscopy shows that monomeric polyglutamine molecules form collapsed structures in aqueous solutions. Proc. Natl. Acad. Sci. USA *103*, 16764–16769.

Dougan, L., Li, J., Badilla, C.L., Berne, B.J., and Fernandez, J.M. (2009). Single homopolypeptide chains collapse into mechanically rigid conformations. Proc. Natl. Acad. Sci. USA *106*, 12605–12610.

Duennwald, M.L., Jagadish, S., Muchowski, P.J., and Lindquist, S. (2006). Flanking sequences profoundly alter polyglutamine toxicity in yeast. Proc. Natl. Acad. Sci. USA *103*, 11045–11050.

Haass, C., and Selkoe, D.J. (2007). Soluble protein oligomers in neurodegeneration: lessons from the Alzheimer's amyloid β-peptide. Nat. Rev. Mol. Cell Biol. *8*, 101–112.

Hatters, D.M. (2008). Protein misfolding inside cells: the case of huntingtin and Huntington's disease. IUBMB Life *60*, 724–728.

Ignatova, Z., and Gierasch, L.M. (2004). Monitoring protein stability and aggregation *in vivo* by real-time fluorescent labeling. Proc. Natl. Acad. Sci. USA *101*, 523–528.

Jackson, G.R., Salecker, I., Dong, X., Yao, X., Arnheim, N., Faber, P.W., MacDonald, M.E., and Zipursky, S.L. (1998). Polyglutamine-expanded human huntingtin transgenes induce degeneration of *Drosophila* photoreceptor neurons. Neuron *21*, 633.

Kaganovich, D., Kopito, R., and Frydman, J. (2008). Misfolded proteins partition between two distinct quality control compartments. Nature *454*, 1088–1095.

Kim, S., Nollen, E.A.A., Kitagawa, K., Bindokas, V.P., and Morimoto, R.I. (2002). Polyglutamine protein aggregates are dynamic. Nat. Cell Biol. *4*, 826–831.

Kopito, R.R. (2000). Aggresomes, inclusion bodies and protein aggregation. Trends Cell Biol. *10*, 524.

Luedtke, N.W., Dexter, R.J., Fried, D.B., and Schepartz, A. (2007). Surveying polypeptide and protein domain conformation and association with FlAsH and ReAsH. Nat. Chem. Biol. *3*, 779–784.

MacDonald, M.E., Ambrose, C.M., Duyao, M.P., Myers, R.H., Lin, C., Srinidhi, L., Barnes, G., Taylor, S.A., James, M., Groot, N., et al. (1993). A novel gene containing a trinucleotide repeat that is expanded and unstable on Huntington's disease chromosomes. Cell *72*, 971–983.

Madani, F., Lind, J., Damberg, P., Adams, S.R., Tsien, R.Y., and Gräslund, A.O. (2009). Hairpin structure of a biarsenical-tetracysteine motif determined by NMR spectroscopy. J. Am. Chem. Soc. *131*, 4613–4615.

Mangiarini, L., Sathasivam, K., Seller, M., Cozens, B., Harper, A., Hetherington, C., Lawton, M., Trottier, Y., Lehrach, H., Davies, S.W., and Bates, G.P. (1996). Exon 1 of the HD gene with an expanded CAG repeat is sufficient to cause a progressive neurological phenotype in transgenic mice. Cell *87*, 493–506.

Matsumoto, G., Kim, S., and Morimoto, R.I. (2006). Huntingtin and mutant SOD1 form aggregate structures with distinct molecular properties in human cells. J. Biol. Chem. *281*, 4477–4485.

Nagai, Y., Inui, T., Popiel, H.A., Fujikake, N., Hasegawa, K., Urade, Y., Goto, Y., Naiki, H., and Toda, T. (2007). A toxic monomeric conformer of the polyglutamine protein. Nat. Struct. Mol. Biol. *14*, 332–340.

Perutz, M.F., Johnson, T., Suzuki, M., and Finch, J.T. (1994). Glutamine repeats as polar zippers: their possible role in inherited neurodegenerative diseases. Proc. Natl. Acad. Sci. USA *91*, 5355–5358.

Rizzo, M.A., Springer, G.H., Granada, B., and Piston, D.W. (2004). An improved cyan fluorescent protein variant useful for FRET. Nat. Biotechnol. *22*, 445–449.

Roberti, M.J., Bertoncini, C.W., Klement, R., Jares-Erijman, E.A., and Jovin, T.M. (2007). Fluorescence imaging of amyloid formation in living cells by a functional, tetracysteine-tagged α-synuclein. Nat. Methods *4*, 345–351.

Rockabrand, E., Slepko, N., Pantalone, A., Nukala, V.N., Kazantsev, A., Marsh, J.L., Sullivan, P.G., Steffan, J.S., Sensi, S.L., and Thompson, L.M. (2007). The first 17 amino acids of huntingtin modulate its sub-cellular localization, aggregation and effects on calcium homeostasis. Hum. Mol. Genet. *16*, 61–77.

Schaffar, G., Breuer, P., Boteva, R., Behrends, C., Tzvetkov, N., Strippel, N., Sakahira, H., Siegers, K., Hayer-Hartl, M., and Hartl, F.U. (2004). Cellular toxicity of polyglutamine expansion proteins: mechanism of transcription factor deactivation. Mol. Cell *15*, 95–105.

Scherzinger, E., Sittler, A., Schweiger, K., Heiser, V., Lurz, R., Hasenbank, R., Bates, G.P., Lehrach, H., and Wanker, E.E. (1999). Self-assembly of polyglutamine-containing huntingtin fragments into amyloid-like fibrils: implications for Huntington's disease pathology. Proc. Natl. Acad. Sci. USA *96*, 4604–4609.

Steffan, J.S., Agrawal, N., Pallos, J., Rockabrand, E., Trotman, L.C., Slepko, N., Illes, K., Lukacsovich, T., Zhu, Y.-Z., Cattaneo, E., et al. (2004). SUMO modification of huntingtin and Huntington's disease pathology. Science *304*, 100–104.

Takahashi, T., Kikuchi, S., Katada, S., Nagai, Y., Nishizawa, M., and Onodera, O. (2008). Soluble polyglutamine oligomers formed prior to inclusion body formation are cytotoxic. Hum. Mol. Genet. *17*, 345–356.

Thakur, A.K., and Wetzel, R. (2002). Mutational analysis of the structural organization of polyglutamine aggregates. Proc. Natl. Acad. Sci. USA *99*, 17014–17019.

Thakur, A.K., Jayaraman, M., Mishra, R., Thakur, M., Chellgren, V.M., Byeon, I.-J., Anjum, D.H., Kodali, R., Creamer, T.P., Conway, J.F., Gronenborn, A.M., and Wetzel, R. (2009). Polyglutamine disruption of the huntingtin exon 1 N terminus triggers a complex aggregation mechanism. Nat. Struct. Mol. Biol. *16*, 380–389.

Wang, Y., Meriin, A.B., Zaarur, N., Romanova, N.V., Chernoff, Y.O., Costello, C.E., and Sherman, M.Y. (2009). Abnormal proteins can form aggresome in yeast: aggresome-targeting signals and components of the machinery. FASEB J. *23*, 451–463.

Zoghbi, H.Y., and Orr, H.T. (2000). Glutamine repeats and neurodegeneration. Annu. Rev. Neurosci. *23*, 217–247.

Zuhlke, C., Rless, O., Bockel, B., Lange, H., and Thies, U. (1993). Mitotic stability and meiotic variability of the $(CAG)_N$ repeat in the Huntington disease gene. Hum. Mol. Genet. *2*, 2063–2067.